Journal of Power Sources 287 (2015) 196–202

Contents lists available at ScienceDirect

Journal of Power Sources

journal homepage: www.elsevier.com/locate/jpowsour

Effect of pretreatment atmosphere on the particle size and oxygen reduction activity of low-loading platinum impregnated titanium carbide powder electrocatalysts

Leerang Yang [a], Yannick C. Kimmel [b], Qi Lu [a, b], Jingguang G. Chen [a, *]

[a] Department of Chemical Engineering, Columbia University, New York, NY 10027, USA
[b] Department of Chemical & Biomolecular Engineering, University of Delaware, Newark, DE 19716, USA

HIGHLIGHTS

- Low-loading Pt/TiC synthesized from impregnation shows high ORR activity.
- The atmosphere during thermal pretreatment affects the Pt particle size and the ORR specific activity.
- Pretreatment of Pt/TiC in H2 leads to smaller Pt particle size and higher ORR activity.
- A surface oxide layer forms on TiC powder after calcination of Pt/TiC in air and results in lower ORR activity.

ARTICLE INFO

Article history:
Received 24 December 2014
Received in revised form
9 March 2015
Accepted 24 March 2015
Available online 6 April 2015

Keywords:
Oxygen reduction reaction
Titanium carbide
Impregnation synthesis
Platinum

ABSTRACT

Low-loading Pt supported on TiC powder catalysts were synthesized by an impregnation method. After the $Pt(NH_3)_4(NO_3)_2$ precursor was impregnated onto the TiC support, different pretreatment atmospheres were used to study the influence on Pt dispersion, surface composition, and catalytic activity towards oxygen reduction reaction (ORR). Direct reduction of the Pt precursor in hydrogen led to small Pt particles with an average size of ~2.2 nm and superior ORR activity at low overpotential compared to commercial Pt/C. However, calcination of the Pt precursor in air resulted in larger Pt particles with an average size of ~6.7 nm and lower ORR specific activity. The decrease in ORR activity was primarily attributed to the surface oxidation of the TiC support during calcination. X-ray photoelectron spectroscopy (XPS) and X-ray diffraction (XRD) confirmed that the TiC powder was oxidized when the catalyst was calcined in air. The finding reported here demonstrates the importance of pretreatment atmosphere for synthesizing Pt-modified transition metal carbides as highly active electrocatalysts.

1. Introduction

The need for active, stable, and inexpensive electrocatalysts has generated interest in high surface area supports that can decrease the use of precious metals without compromise in activity [1]. Transition metal carbides (TMCs) are one promising class of support materials, which often show similar chemical and electronic properties to Pt-group metals [2]. Many transition metal carbides exhibit high chemical stability, resistance to corrosion and poisoning, and high electric conductivity [3]. As summarized in recent reviews [3,4], many recent studies have utilized low-loading platinum supported on transition metal carbides as electrocatalysts for various applications, such as the hydrogen evolution reaction (HER) [5,6] and oxygen reduction reaction (ORR) [7].

Our group has previously reported that a monolayer of Pt on titanium carbide (TiC) thin film exhibited similar HER activity as bulk Pt, which was attributed to similar hydrogen binding energies between Pt/TiC and Pt from density functional theory (DFT) calculations [8]. This result was extended to Pt supported TiC powders which showed same activity as a much higher loading of Pt supported on carbon powder, the conventional electrocatalyst used in a PEM fuel cell and electrolyzer [8]. TiC is an attractive catalyst support because it can be synthesized at a relatively low

* Corresponding author.
E-mail address: jgchen@columbia.edu (J.G. Chen).

http://dx.doi.org/10.1016/j.jpowsour.2015.03.146
0378-7753/

temperature that results in a high surface area, which is necessary for commercial use [9]. Additionally, TiC is useful as a support for low loading Pt compared to carbon because TiC can stabilize Pt, preventing Pt agglomeration that leads to the loss of active Pt surface area exhibited on carbon [1] and [10]. DFT calculations of binding energies of Pt–Pt, Pt–C and Pt–TiC showed that a Pt atom is more stable to bond to a TiC surface rather than to another Pt atom, while a Pt atom is more favorable to bond to another Pt atom rather than to graphite [8]. Lastly, it has been demonstrated that TiC is electrochemically stable over a wide range of pH, thus is a suitable support for many electrochemical reactions [11]. This includes the oxygen reduction reaction (ORR), which occurs under conditions that are generally too oxidizing for most other transition metal carbides.

While TMCs are promising supports for Pt-group metals, currently there is a lack of detailed studies of optimal conditions on the synthesis of low loadings of Pt supported on TMC powders. Generally, supported metal powder catalysts can be synthesized from several methods including impregnation, reductive deposition precipitation, colloidal precipitation, and electrodeposition [12]. For high metal loadings, colloidal precipitation [12] or chemical reduction [13] methods are often preferred in order to achieve high dispersion and precise control over the size of the metal nanoparticles. Previous studies of Pt supported on TiC and its derivatives, such as titanium oxycarbides or $Ti_3C_2X_2$ (X = OH, F), utilized chemical reduction [14,15] or electrodeposition [16] to synthesize relatively high-loading Pt catalysts. However, for lower metal loadings, impregnation is favored because it is a direct and low-cost synthesis method.

The impregnation method must be followed by a thermal pretreatment to decompose the metal precursor. The pretreatment parameters such as temperature and gaseous atmosphere, *e.g.*, oxidizing or reducing, affect the surface composition, morphology, and catalytic performance of the metal catalysts [17,18]. Additionally, thermal pretreatment in oxygen-containing environment can lead to surface oxidation of the transition metal carbide support [19]. In such case, the resulting Pt particles are supported on a transition metal oxide shell encapsulating a metal carbide core, rather than just the metal carbide itself. Consequently, the surface electronic properties and metal-support interaction deviate from the behaviors of the oxide-free support [20,21].

The main focus of this study was to synthesize and demonstrate the catalytic activity of low-loading Pt supported on TiC powder, and to explore how the thermal decomposition atmosphere of Pt precursor affects the ORR activities. Specifically, Pt precursor was impregnated on TiC powders and decomposed under three different gas-phase conditions: Air (oxidizing environment), hydrogen (reducing environment), and a successive sequence of air and hydrogen (oxidizing followed by a reducing environment). The Pt modified TiC powders were characterized with X-ray diffraction (XRD), X-ray photoelectron spectroscopy (XPS), and transmission electron microscopy (TEM). Copper underpotential deposition (UPD) was used to determine the electrochemically active surface area of Pt/TiC. The ORR was used as a probe reaction to test the activities of the synthesized powders. Results indicate that pretreatment atmosphere greatly influences the catalytic activity by affecting the surface oxidation and Pt particle size. Pt/TiC powders synthesized under a reducing environment, without leading to excess surface oxidation of the TiC support, demonstrate high ORR activity. In contrast, Pt/TiC powders calcined in air show a surface oxide layer and a poor Pt dispersion, which adversely affect the ORR activity of the catalysts. Although the study is carried out on TiC, the general findings of the effect of pretreatment procedures should be useful for synthesizing low loadings of Pt on other transition metal carbide supports.

2. Experimental methods

2.1. Synthesis

TiC powder (30–50 nm APS Powder, S.A. 35–45 $m^2\ g^{-1}$) was purchased from Alfa Aesar and used as received. The TiC powder was impregnated with Pt (1.75 wt%) by using 0.018 M tetraammineplatinum(II) nitrate ($Pt(NH_3)_4(NO_3)_2$) as a precursor dissolved in deionized water. The slurry was stirred at room temperature for 12 h to ensure the adsorption of precursor onto the TiC surface, and the solvent was slowly evaporated at 55 °C for ~12 h. The solid product was further dried in air by increasing the temperature to 100 °C at a rate of 0.4 °C min^{-1} and drying at 100 °C for 10 h. After the solid product was cooled and finely ground, three different pretreatment methods were used to decompose the adsorbed Pt precursor. For the first method, the product was calcined in air. The powders were heated at a rate of 2.0 °C min^{-1} to 290 °C and held at 290 °C for 2 h [22]. The catalyst produced from this method will be referred to as Pt/TiC(Air) for the remainder of this manuscript. For the second method, the dried product was directly reduced under hydrogen at a flow rate of 100 sccm (standard cubic centimeter per minute) in a quartz tube furnace. The temperature was increased to 310 °C at a ramp rate 1.0 °C min^{-1}, and then held at 310 °C for 5 h. After the furnace cooled to room temperature, the powder was passivated under an atmosphere of 99% N_2 and 1% O_2 (total flow rate 20 sccm) for 1 h. The catalyst produced from the second method will be referred to as Pt/TiC(H_2). For the third method, the dried product was first calcined in an identical manner to the first method. After the calcination, it was successively reduced in hydrogen at 310 °C for 3 h and passivated at room temperature in a similar manner to the second method. The catalyst produced from this method will be referred to as Pt/TiC(Air|H_2).

2.2. Material characterization

For surface composition studies, XPS measurements were performed with a Phi 5600 XPS system using an Al X-ray source. For the bulk crystallographic information, powder XRD was performed using a PANalytical X'Pert diffractometer with a Cu Kα radiation at 45 kV and 40 mA. TEM measurements were obtained employing a JEOL JEM-2010F using an accelerating voltage of 200 kV.

2.3. Electrode preparation

For each Pt/TiC catalyst ink and unmodified TiC, 78 mg of the catalyst was dispersed in 5 mL of ethylene glycol and sonicated for at least 40 min. A total of 30 μL of ink was deposited onto a glassy carbon electrode (0.196 cm^2, Pine Research Instrumentation) by pipetting of 10 μL ink onto the electrode and subsequent drying in air at 100 °C three times. For Pt/TiC catalysts, the final platinum loading on the glassy carbon electrode was 0.041 mg cm^{-2}_{disk}. For reference, commercial 40% Platinum on Vulcan XC-72 carbon (Premetek) ink was prepared by mixing 3.4 mg of Pt/C catalyst in 5 ml of ethylene glycol and depositing on the glassy carbon electrode in an identical manner. After the Pt/TiC and Pt/C inks were dried completely, 3 μL of ~5% Nafion 117 solution (Sigma–Aldrich) was dropped on top of the electrodes to act as a binder [23].

2.4. Electrochemical characterization

A standard three-electrode setup was used for all electrochemical characterization. Along with the prepared working electrodes, a saturated calomel electrode (SCE, Pine Research Instrumentation) was used as the reference electrode and a Pt wire (Alfa Aesar, 99.99%) was used as the auxiliary electrode. For

activation of the catalysts, the working electrodes were first cycled in argon-saturated 0.5 M sulfuric acid for 60 cycles, at a rate of 0.1 V s^{-1}, between 0.0 V and 1.2 V for Pt/C and between 0.0 V and 1.0 V for the Pt/TiC catalysts. All potentials are reported with respect to normal hydrogen electrode (NHE).

For ORR experiments, the activated electrodes were first cycled in oxygen-saturated 0.5 M sulfuric acid for 5 cycles in the same manner as the activation step. Subsequently, a linear scan voltammetry (LSV) measurement was performed at room temperature from 1.0 V to 0.0 V, with a sweep rate of 0.01 Vs^{-1}. During the LSV, electrodes were rotated at 400, 900, 1600, and 2500 rpm to control the mass transport of oxygen to the surface.

The Cu UPD stripping method was used to estimate the electrochemically active surface area (ECSA) of Pt for each sample. The hydrogen adsorption/desorption charge method [24], a commonly used method for calculating ECSA, was not appropriate for Pt/TiC samples because of background hydrogen adsorption onto the TiC support. For Cu UPD stripping, the electrodes were first cleaned in Ar-saturated 0.1 M H_2SO_4 solution for 60 cycles in a similar manner to the cleaning procedure described above. A background sweep was performed by holding the electrode potential at 0.317 V vs. NHE for 120 s and then sweeping to 0.942 V at a rate of 0.1 V s^{-1}. Subsequently, an identical LSV scan was repeated in an electrolyte of 0.1 M H_2SO_4 + 3 mM $CuSO_4$ to measure the underpotential deposition and stripping of monolayer copper from the Pt surface. The total charge transferred from the Cu UPD stripping (Q_{Cu}) was calculated from the current difference between the two curves. Electrochemical surface area (ECSA) was then calculated by dividing Q_{Cu} by 420 μC cm^{-2}, the standard value of charge transfer for monolayer Cu deposited on polycrystalline Pt [25].

3. Results and discussion

3.1. Material characterization

3.1.1. XPS measurements

The Pt 4f regions of Pt/TiC samples (Fig. 1a) confirm the presence of Pt on the Pt/TiC catalysts. The XPS peaks at 71.1 eV ($4f_{7/2}$) and 74.4 eV ($4f_{5/2}$) for Pt/TiC(H_2) and Pt/TiC(Air|H_2) samples are assigned to the metallic Pt. For Pt/TiC(Air), however, the binding energies of the Pt 4f peaks are shifted to higher values because of oxidation. For Pt/TiC(Air), the small shoulder at 72.0 eV is assigned to PtO, while the two peaks at 74.1 eV and 77.8 eV are assigned to PtO_2 [26]. The XPS results suggest that Pt was oxidized during calcination for Pt/TiC(Air) and Pt/TiC(Air|H_2), but for the latter, the subsequent reduction in hydrogen reduced the oxidized Pt to metallic Pt. Notably, despite the same platinum loading, the XPS peak area ratio of Pt 4f to Ti 2p is significantly higher for Pt/TiC(H_2) than for Pt/TiC(Air) and Pt/TiC(Air|H_2), as shown in Table 1. This indicates a higher dispersion of Pt on Pt/TiC(H_2) than on the other two samples [27].

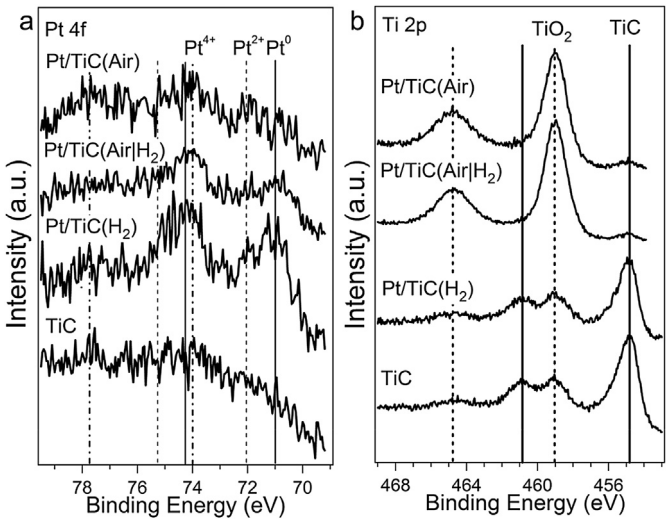

Fig. 1. XPS spectra of (a) Pt 4f, (b) Ti 2p.

As shown in Fig. 1b, the Ti $2p_{3/2}$ and $2p_{1/2}$ region of Pt/TiC(H_2) shows peaks that are assigned to the carbidic Ti, at 454.8 eV and 461.1 eV [28]. The passivated surface gives rise to two peaks at higher energies, 459.0 eV and 464.5 eV, which correspond to TiO_2 [29]. The Ti 2p region of Pt/TiC(Air) and Pt/TiC(H_2|Air) have two dominant TiO_2 peaks and only a trace of carbidic Ti peak at 454.9 eV, indicating that the surfaces of those TiC powders are nearly completely oxidized.

3.1.2. XRD analysis

The XRD patterns of Pt/TiC samples are shown in Fig. 2. All peaks were identified using the JCPDS database: Pt(65–2868), TiC(65–8417), and anatase TiO_2(21–1272). For Pt/TiC(H_2), pattern (c), no bulk TiO_2 was detected. For Pt/TiC(Air) and Pt/TiC(Air|H_2), pattern (a) and (b) respectively, the relative intensities of peaks show that approximately 15% of the TiC was oxidized to anatase TiO_2 . This suggests that the TiC surface was oxidized when Pt/TiC(Air) and Pt/TiC(Air|H_2) powders were calcined in air at the temperature of 290 °C. This temperature is about 50 °C above the minimum temperature needed for the thermal decomposition of the precursor, $Pt(NH_3)_4(NO_3)_2$ [18]. Both XPS and XRD spectra of Pt/TiC(Air|H_2) show that the consequent reduction in hydrogen at 310 °C after calcination did not reduce the extent of Ti oxidation in this sample.

3.1.3. TEM results

The TEM images in Fig. 3 show the morphology of Pt particles on the Pt/TiC powders. The average Pt particle size in the catalysts was greatly influenced by the decomposition environment of the Pt precursor. Samples that were calcined in air, Pt/TiC(Air) (Fig. 3a) and Pt/TiC(Air|H_2) (Fig. 3b), showed larger Pt particles than those of the sample reduced in hydrogen, Pt/TiC(H_2). The Pt particles on both Pt/TiC(Air) and Pt/TiC(Air|H_2) were characterized by average diameters of 6.7 ± 1.2 nm. Low dispersion of Pt after decomposition of precursor in an oxidizing environment has been attributed to the fast rate of decomposition, which allows the first formed Pt nuclei to grow into large particles before other nuclei can form [18]. Another factor that may contribute to the large particle size is the formation of mobile PtO_x species during calcination [30]. The observation of similar particle size between the Pt/TiC(Air) and Pt/TiC(Air|H_2) samples indicates that the initial decomposition of the precursor was the crucial step for determining the platinum particle size, which was not altered by subsequent treatment in hydrogen. By contrast, Pt/TiC(H_2) (Fig. 3c) shows highly dispersed platinum particles with an average particle size of 2.2 ± 0.7 nm, similar to the Pt particles sizes of the commercial Pt/C catalysts [24].

3.1.4. UPD Cu stripping

The ECSAs of the samples were determined from UPD Cu

Table 1
XPS peak area ratio between Pt 4f and Ti 2p region for the prepared Pt/TiC samples.

	Pt/TiC(Air)	Pt/TiC(Air|H_2)	Pt/TiC(H_2)
Pt 4f/Ti 2p	0.063	0.054	0.083

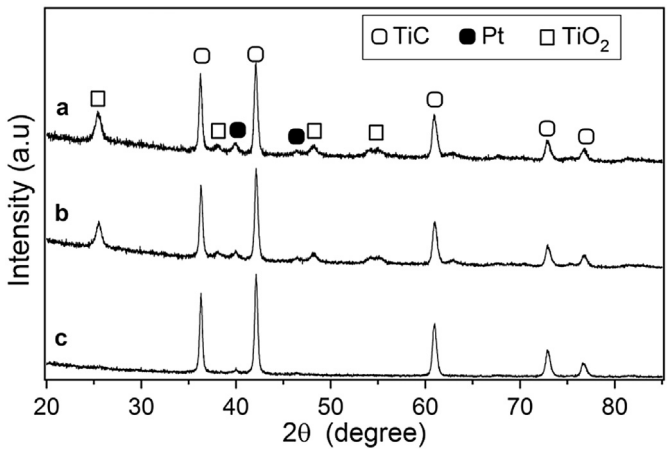

Fig. 2. XRD patterns of (a) Pt/TiC(Air), (b) Pt/TiC(Air|H_2), and (c) Pt/TiC(H_2).

stripping. In Fig. 4, UPD Cu stripping currents are shown in tandem with background currents. The stripping current for the Pt/C catalyst, Fig. 4e, displays a typical UPD Cu stripping current for polycrystalline Pt, showing that the Cu monolayer desorption occurs in several steps rather than in a single step [31]. The first well-defined peak at 0.42 V corresponds to Pt(100), and the second well-defined peak at 0.60 V corresponds to the additional Cu desorption from the three low-index facets, *i.e.* Pt(100), Pt(111), and Pt(110) [31]. The Pt/TiC samples show Cu stripping currents at the same potential range. The charge transferred, Q_{Cu}, and the corresponding ECSAs are summarized in Table 2. Pt/TiC(Air) and Pt/TiC(Air|H_2) both show significantly lower ECSA than Pt/TiC(H_2), consistent with the TEM observation of larger average Pt particles in the former two catalysts. Moreover, the reduction of ECSA has been reported for TiO_2 supported electrocatalysts due to the low electric conductivity of bulk TiO_2 [32,33]. Hence, the formation of the TiO_2 layer on the surface of TiC supports may also contribute to the low ECSA of Pt/TiC(Air) and Pt/TiC(Air|H_2).

Another important point from Table 2 is that the Pt/C electrode has *c.a.* 2.3 times higher ECSA than the Pt/TiC(H_2) electrode. Based on the TEM observation of similar Pt particle sizes on Pt/TiC(H_2) and commercial Pt/C catalysts, the difference in ECSA is likely due to the large discrepancy in catalyst loading. While both electrodes have 0.041 mg cm^{-2}_{disk} Pt loading, the actual catalyst loading is 0.10 mg cm^{-2}_{disk} for 40% Pt/C and 2.3 mg cm^{-2}_{disk} for Pt/TiC. The thinner catalyst film on the Pt/C electrode allows the majority of the Pt particles to be in contact with the electrolyte and participate in electrochemical reactions. The Pt/TiC electrode, however, is covered with a thicker catalyst film, and some Pt particles inside the film are not exposed to the electrolyte solution [24], resulting in the lower ECSA of the Pt/TiC electrodes.

This discrepancy presents an intrinsic challenge for using an RDE setup to compare the catalysts with large Pt loading differences, as mass activities can be compared only with an assumption that same amount of Pt is actually participating in the reaction. Therefore, in this paper, ECSA-normalized specific activities are compared between the Pt/C and the Pt/TiC samples.

3.2. ORR activity

Several parameters were used to assess the performance of the catalysts towards ORR: the oxygen reduction peak potential in CV, the half-wave potential of LSV, the kinetic current densities at 0.88 V and 0.83 V vs. NHE (0.90 V and 0.85 V vs. RHE), and the number of electrons transferred at the rate determining step calculated from the Koutecky–Levich plot.

3.2.1. CV under inert and oxygen conditions

Fig. 5 shows the CVs measured in O_2-saturated 0.5 M H_2SO_4 (solid line) and in Ar-saturated 0.5 M H_2SO_4 (dotted line). The reduction peaks were observed at negative CV scans for all tested catalysts. The Pt/TiC samples did not display Pt reduction peaks in the Ar-saturated CV due to their low Pt loadings. For Pt/C, the reduction peak at 0.73 V in the Ar-saturated electrolyte is assigned to Pt reduction, and the reduction peak at 0.77 V in the O_2-saturated electrolyte is the mixed potential of Pt reduction and oxygen reduction. For CV measurements of ORR kinetics, the closer the peak location is to the reversible O_2 potential at 1.2 V, the easier for ORR to occur on the catalyst surface. Among the Pt/TiC catalysts, Pt/TiC(H_2) showed the most positive oxygen reduction peak potential at 0.73 V. For Pt/TiC(Air) and Pt/TiC(Air|H_2), peaks were at significantly more negative potentials, 0.61 V and 0.65 V, respectively.

3.2.2. ORR LSV

Similar trends in activity were also found with LSV. Fig. 6 compares the ORR performance of the Pt/TiC and Pt/C electrodes in O_2-saturated 0.5 M H_2SO_4 solution. As seen in the LSV curves, the contribution of bare TiC support was negligible in the potential region above 0.6 V. Therefore the reaction can be considered to occur only on Pt surface between 0.6 and 1.0 V. Pt/TiC(H_2), with the half-wave potential of 0.78 V, exhibited a superior ORR activity compared to Pt/TiC(Air) and Pt/TiC(Air|H_2), both of which showed a half-wave potential of 0.68 V. The CV peak potentials and the half-wave potentials are summarized in Table 3.

The Pt/C electrode showed the most positive half-wave potential. This, however, cannot be directly compared to the Pt/TiC samples due to differences in the ECSA, as previously discussed in the Section 3.2.1. More direct comparison of intrinsic kinetic

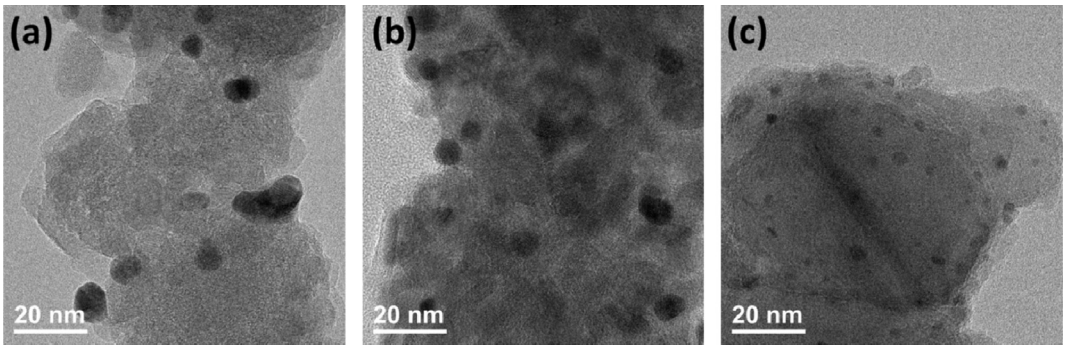

Fig. 3. TEM images of Pt/TiC samples. (a) Pt/TiC(Air), (b) Pt/TiC(Air|H_2), (c) Pt/TiC(H_2).

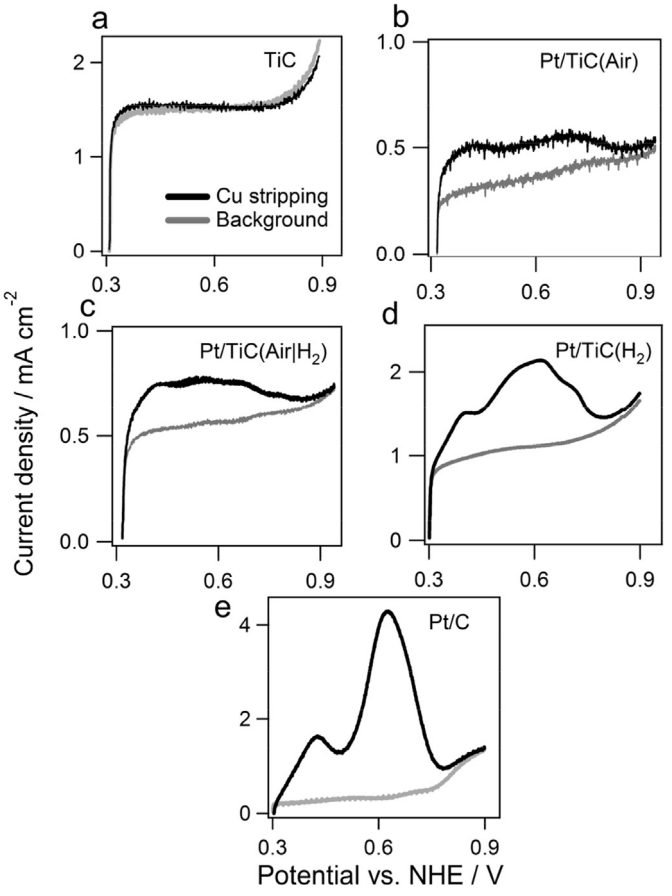

Fig. 4. Cu UPD stripping result with background, (a) TiC, (b) Pt/TiC(Air), (c) Pt/TiC(Air|H_2), (d) Pt/TiC(H_2), and (e) Pt/C.

Table 2
Charges transferred during the Cu stripping, and the electrochemically active surface area calculated accordingly from the Cu stripping experiment.

	Pt/C	Pt/TiC(H_2)	Pt/TiC(Air)	Pt/TiC(Air|H_2)
Q_{Cu} (mC $cm^{-2}{}_{disk}$)	8.1	3.5	0.81	1.1
ECSA (m^2 $g^{-1}{}_{Pt}$)	47	20	4.7	6.4

activities is made by calculating the kinetic current density j_k from the Levich equation [34]:

$$j_k = \frac{j_l \times j}{j_l - j}$$

where j_i is the limiting current density and j is the measured current density. Fig. 7 displays the kinetic current densities normalized by the ECSA.

When normalized to ECSA, Pt/TiC(H_2) had the highest specific activity in the shown region among all tested samples, including Pt/C. The improved activity of Pt/TiC(H_2) compared to Pt/C was especially evident at the low overpotential region. At 0.9 V, the specific activity was 40% higher than that of the Pt/C catalyst. However, Pt/TiC(H_2) also had a higher Tafel slope compared to that of Pt/C, therefore the ORR activities of the two samples eventually converged at ~0.85 V. The specific kinetic activities of the four catalysts at 0.88 V and 0.83 V vs. RHE are compared in Fig. 8. The kinetic current densities were calculated by averaging the results measured at 400 rpm, 900 rpm, 1600 rpm, and 2500 rpm.

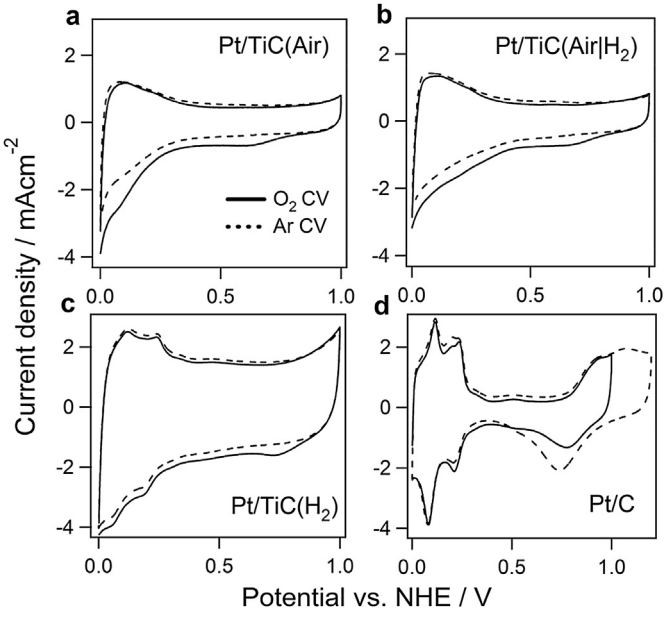

Fig. 5. CVs of (a) Pt/TiC(Air), (b) Pt/TiC(Air|H_2), (c) Pt/TiC(H_2), and (d) Pt/C in Ar-saturated 0.5 M H_2SO_4 (dotted line, 60th cycle shown) and O_2-saturated 0.5 M H_2SO_4 (solid line, 5th cycle shown). All CVs were recorded at room temperature and a scan rate of 0.1 V s^{-1}.

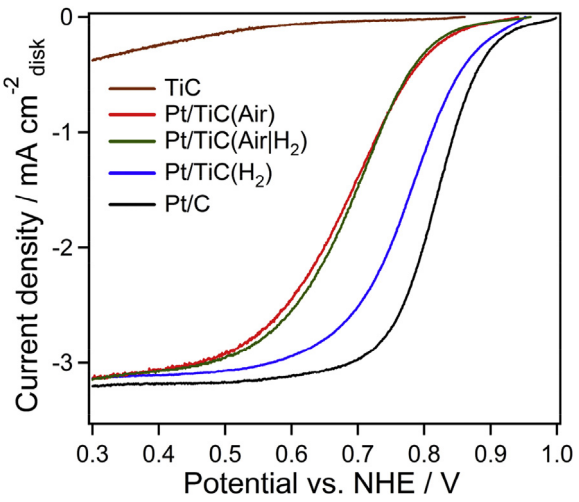

Fig. 6. LSV of Pt/TiC(Air), Pt/TiC(Air|H_2), Pt/TiC(H_2), Pt/C, and TiC in O_2 saturated 0.5 M H_2SO_4 solution, measured at a rotation rate of 1600 rpm and a scan rate of 0.01 V s^{-1}.

Table 3
ORR parameters of Pt/C and Pt/TiC catalysts.

	CV peak (V/NHE)	$E_{1/2}$ (V/NHE)
Pt/C	0.77	0.81
Pt/TiC(H_2)	0.73	0.78
Pt/TiC(Air)	0.62	0.68
Pt/TiC(Air|H_2)	0.65	0.68

Compared to Pt/TiC(H_2), the Pt/TiC(Air) and Pt/TiC(Air|H_2) samples showed significantly lower specific activities. Pt/TiC(Air) and Pt/TiC(Air|H_2) showed specific kinetic current densities 30–40% lower than that of Pt/TiC(H_2) at both potentials. This is an intriguing finding because it is opposite to what the particle size

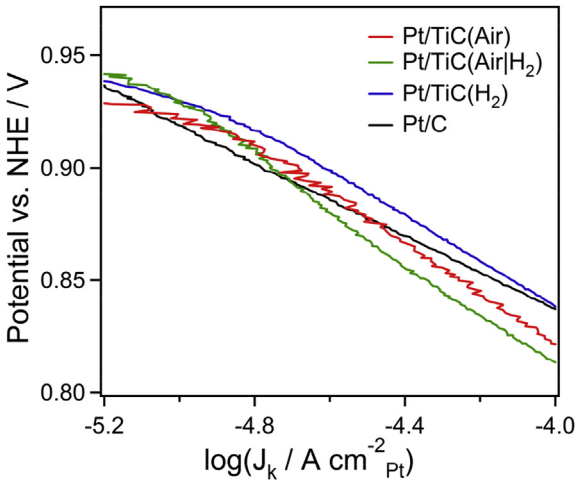

Fig. 7. Kinetic current densities normalized to ECSA, measured in O_2-saturated 0.5 M H_2SO_4, room temperature, and rotation rate 1600 rpm.

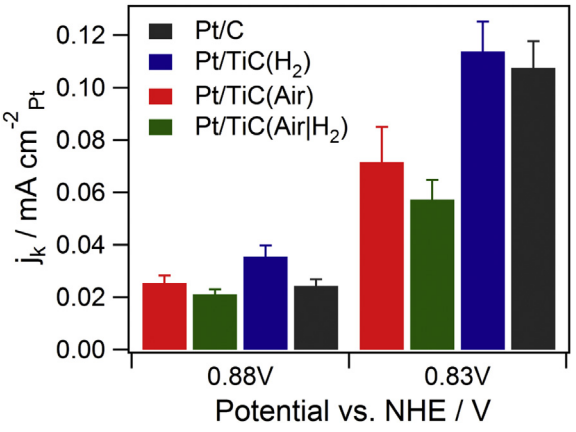

Fig. 8. ORR kinetic current densities of the prepared supported Pt powders at 0.88 V and 0.83 V vs. NHE, normalized to ECSA.

effect predicts for catalysts with different Pt particle sizes. The particle size effect for ORR on Pt catalysts has been well studied both experimentally and theoretically [35–37]. Shao et al., in particular, used an RDE setup similar to the experimental method presented herein to test the particle size effect [36]. There is a general agreement that the specific ORR activity increases as the Pt particle size increases, due to the much higher ORR activity on Pt(100) than on Pt(111). Therefore, the low ORR specific activities of Pt/TiC(Air) and Pt/TiC(Air|H_2), despite large Pt particle sizes, imply that there should be other factors that adversely affect the activities of the two samples.

The major difference between Pt/TiC(H_2) and the two calcined samples is the surface composition. XPS results indicate high contents of TiO_2 on the surfaces of Pt/TiC(Air) and Pt/TiC(Air|H_2) resulting from the calcination. The decreased ORR activity suggests that the surface oxidation of the TiC support inhibits the metal-support interaction between Pt and transition metal carbides that might lead to a higher ORR activity as observed for Pt/TiC(H_2). Such a hypothesis is supported by the observation made by Liu and Mustain when comparing the ORR activity of Pt/WC to Pt/WO_3; Pt/WC showed a significantly higher ORR activity and selectivity for the desired 4 electron pathway than Pt/WO_3 [38].

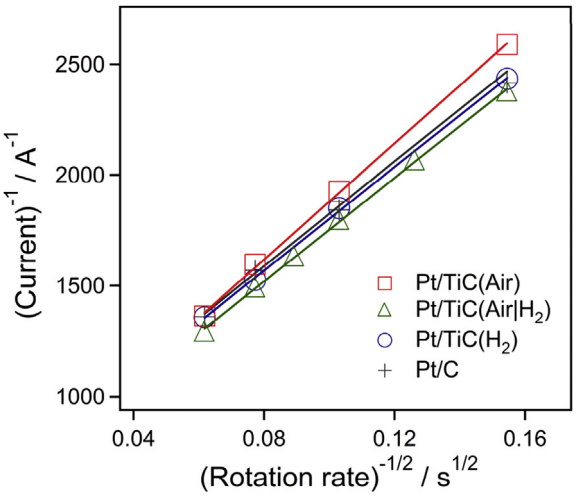

Fig. 9. Koutecky–Levich plots for the ORR catalysts in 0.5 M H_2SO_4.

3.2.3. *Koutecky–Levich analysis*

The limiting current densities at several different disk rotation speeds were used to construct the Koutecky–Levich plots in Fig. 9. These plots relate limiting current densities and the rotation speeds of the RDE, based on the principle that measured current (i) is related to the kinetic current (i_k) and the limiting current (i_l) as described in equation (1):

$$\frac{1}{i} = \frac{1}{i_k} + \frac{1}{i_l} = \frac{1}{i_k} + \frac{1}{B\omega^{1/2}} \quad (1)$$

The slope of the Koutecky–Levich plot, B, is defined as follows:

$$B = 0.62nFAD_{O_2}^{2/3}\nu^{-1/6}C_{O_2}$$

Where F = Faraday constant, D_{O_2} = oxygen diffusion coefficient, ν = kinematic viscosity of the solution, C_o = oxygen solubility in the electrolyte, and A = geometric area of electrode. Using this equation, the number of electrons transferred (n) can be calculated.

As shown in Fig. 9, good linear relationships were observed for all four catalysts. It is well known that the oxygen reduction occurs through a 4 electron pathway on 40% Pt/C in 0.5 M H_2SO_4 electrolyte [39]. Therefore, by setting n = 4 for the Pt/C catalyst, the number of electrons transferred were calculated as 3.4 for Pt/TiC(Air), and 3.9 for both Pt/TiC(H_2) and Pt/TiC(Air|H_2). This indicates that ORR takes place predominantly via the direct 4-electron pathway on Pt/TiC(H_2) as well as Pt/TiC(Air|H_2). For Pt/TiC(Air), however, significant amount of the 2-electron H_2O_2 byproduct is produced. Based on the results of XPS, XRD, and TEM, the most notable difference between Pt/TiC(Air) and PtTiC(Air|H_2) was the oxidation state of Pt, while the Pt particle size and the bulk crystallinity were similar for the two samples.

4. Conclusions

Low-loading Pt/TiC catalysts were synthesized with an impregnation method, and the influence of the gas-phase pretreatment environment was studied. Two important findings are presented in this paper.

(1) The Pt particle sizes on the synthesized Pt/TiC catalysts were greatly dependent on the thermal pretreatment environment. When the Pt precursor impregnated on TiC was thermally decomposed in H_2, Pt was highly dispersed on the

support surface with the average size of ~2.2 nm. In contrast, when the Pt precursor was calcined in an oxygen environment, the average Pt particle size on TiC was around ~6.7 nm, resulting in lower ECSA.

(2) The surface oxidation, for both Pt and TiC, affected the ORR activity and selectivity. Pt/TiC(H_2) was synthesized without excessive surface oxidation of the support and showed an improved ORR specific activity compared to Pt/C. In contrast, Pt/TiC(Air) and Pt/TiC(Air|H_2) showed lower ORR activity than Pt/TiC(H_2), suggesting that the formation of the support oxide layer adversely affects the catalytic activity. Moreover, it was determined from the Koutecky–Levich analysis that Pt/TiC(Air) reduces significant portion of oxygen via the 2-electron pathway, which may be attributed to the oxidized surface of the Pt particles.

Acknowledgments

The authors acknowledge support from the Department of Energy, Office of Basic Energy Sciences (Grant #DE-FG02-13ER16381).

References

[1] Y. Shao, J. Liu, Y. Wang, Y. Lin, J. Mater. Chem. 19 (2009) 46–59.
[2] H.H. Hwu, J.G. Chen, Chem. Rev. 105 (2005) 185–212.
[3] Y. Liu, T.G. Kelly, J.G. Chen, W.E. Mustain, ACS Catal. 3 (2013) 1184–1194.
[4] T.G. Kelly, J.G. Chen, Chem. Soc. Rev. 41 (2012) 8021–8034.
[5] C. Ma, J. Sheng, N. Brandon, C. Zhang, G. Li, Int. J. Hydrog. Energy 32 (2007) 2824–2829.
[6] D.V. Esposito, S.T. Hunt, A.L. Stottlemyer, K.D. Dobson, B.E. McCandless, R.W. Birkmire, J.G. Chen, Angew. Chem. Int. Ed. 49 (2010) 9859–9862.
[7] I.J. Hsu, D.A. Hansgen, B.E. McCandless, B.G. Willis, J.G. Chen, J. Phys. Chem. C 115 (2011) 3709–3715.
[8] Y.C. Kimmel, L. Yang, T.G. Kelly, S.A. Rykov, J.G. Chen, J. Catal. 312 (2014) 216–220.
[9] D.W. Flaherty, R.A. May, S.P. Berglund, K.J. Stevenson, C.B. Mullins, Chem. Mater. 22 (2009) 319–329.
[10] J. Liu, Z. Zhou, X. Zhao, Q. Xin, G. Sun, B. Yi, Phys. Chem. Chem. Phys. 6 (2004) 134–137.
[11] Y.C. Kimmel, X. Xu, W. Yu, X. Yang, J.G. Chen, ACS Catal. 4 (2014) 1558–1562.
[12] W. Yu, M.D. Porosoff, J.G. Chen, Chem. Rev. 112 (2012) 5780–5817.
[13] P. Kim, J.B. Joo, W. Kim, J. Kim, I.K. Song, J. Yi, J. Power Sources 160 (2006) 987–990.
[14] X. Xie, S. Chen, W. Ding, Y. Nie, Z. Wei, Chem. Commun. 49 (2013) 10112–10114.
[15] K. Huang, Y. Li, Y. Xing, J. Mater. Res. 28 (2013) 454–460.
[16] Y. Ou, X. Cui, X. Zhang, Z. Jiang, J. Power Sources 195 (2010) 1365–1369.
[17] J. Santos, J. Phillips, J.A. Dumesic, J. Catal. 81 (1983) 147–167.
[18] M.K. Oudenhuijzen, P.J. Kooyman, B. Tappel, J.A. van Bokhoven, D.C. Koningsberger, J. Catal. 205 (2002) 135–146.
[19] J. Polonský, I. Petrushina, E. Christensen, K. Bouzek, C.B. Prag, J.E.T. Andersen, N.J. Bjerrum, Int. J. Hydrog. Energy 37 (2012) 2173–2181.
[20] M. Nakazawa, H. Okamoto, Appl. Surf. Sci. 24 (1985) 75–86.
[21] H. Chhina, S. Campbell, O. Kesler, J. Power Sources 164 (2007) 431–440.
[22] F. Pinna, Catal. Today 41 (1998) 129–137.
[23] U. Paulus, T. Schmidt, H. Gasteiger, R. Behm, J. Electroanal. Chem. 495 (2001) 134–145.
[24] A. Pozio, M. De Francesco, A. Cemmi, F. Cardellini, L. Giorgi, J. Power Sources 105 (2002) 13–19.
[25] C.L. Green, A. Kucernak, J. Phys. Chem. B 106 (2002) 1036–1047.
[26] H. Hagiwara, M. Nagatomo, C. Seto, S. Ida, T. Ishiahara, Catal. 3 (2013) 614–624.
[27] B.M. Reddy, B. Chowdhury, P.G. Smirniotis, Appl. Catal. A-Gen. 211 (2001) 19–30.
[28] M.C. Biesinger, L.W. Lau, A.R. Gerson, R.S.C. Smart, Appl. Surf. Sci. 257 (2010) 887–898.
[29] B. Erdem, R.A. Hunsicker, G.W. Simmons, E.D. Sudol, V.L. Dimonie, M.S. El-Aasser, Langmuir 17 (2001) 2664–2669.
[30] A. Borgna, T.F. Garetto, C.R. Apesteguı, F. Le Normand, B. Moraweck, J. Catal. 186 (1999) 433–441.
[31] D.M. Kolb, R. Kötz, K. Yamamoto, Surf. Sci. 87 (1979) 20–30.
[32] S. von Kraemer, K. Wikander, G. Lindbergh, A. Lundblad, A.E.C. Palmqvist, J. Power Sources 180 (2008) 185–190.
[33] C. Gebauer, Z. Jusys, M. Wassner, N. Hüsing, R.J. Behm, ChemPhysChem 15 (2014) 2094–2107.
[34] A.J. Bard, L.R. Faulkner, Electrochemical Methods: Fundamentals and Applications, Wiley, New York, 1980.
[35] K. Kinoshita, J. Electrochem. Soc. 137 (1990) 845–848.
[36] M. Shao, A. Peles, K. Shoemaker, Nano Lett. 11 (2011) 3714–3719.
[37] M. Peuckert, H. Bonzel, Surf. Sci. 145 (1984) 239–259.
[38] Y. Liu, W.E. Mustain, ACS Catal. 1 (2011) 212–220.
[39] J. Perez, E.R. Gonzalez, E.A. Ticianelli, Electrochim. Acta 44 (1998) 1329–1339.